IEEE Access
Multidisciplinary | Rapid Review | Open Access Journal

Received March 7, 2019, accepted March 22, 2019, date of publication March 29, 2019, date of current version April 19, 2019.

Digital Object Identifier 10.1109/ACCESS.2019.2907742

W-Band Near-Field Microscope

GUANGBIN DAI[1,2], GUOSHUAI GENG[1], XIAOXUAN ZHANG[1], JIE WANG[1,2], TIANYING CHANG[1], AND HONG-LIANG CUI[1,2]

[1]College of Instrumentation and Electrical Engineering, Jilin University, Changchun 130061, China
[2]Center of Applied Physics, Chongqing Institute of Green and Intelligent Technology, Chinese Academy of Sciences, Chongqing 400714, China

Corresponding author: Tianying Chang (tchang@jlu.edu.cn)

This work was supported in part by the National Key Research and Development Program of China under Grant 2017YFF0106303, Grant 2016YFC0101002, and Grant 2016YFC0101301, in part by the Central Government Supported Key Instrument Program of China under Grant YXGYQ201700136, in part by the National Natural Science Foundation of China under Grant 61875196 and Grant 11604332, in part by the Chongqing Science and Technology Commission under Grant cstc2018jcyjAX0405, and in part by the Chinese Academy of Sciences for a Key Scientific Instrument and Equipment Development Project.

ABSTRACT A home-built scattering-type scanning near-field millimeter-wave microscope based on a 110-GHz continuous-wave solid-state source is demonstrated with a spatial resolution of 1 μm, approximately 1/3000 of the incident wavelength, and a signal-to-noise ratio of 23.8 dB. The relationship between the length of the tip (antenna) and the wavelength for resonant enhancement, and the near-field distribution around the tip apex at different tip-sample separations were explored using finite-difference time-domain electromagnetic simulations to facilitate the design of the microscope. The dependence of the spatial resolution on the tip-sample separation and the harmonic order of the modulation frequency at which the near-field signal was extracted has been investigated experimentally and discussed in terms of the signal-to-noise ratio and the standard deviation of the demodulated signal.

INDEX TERMS Millimeter wave, near-field, FDTD, high resolution, background noise.

I. INTRODUCTION

Limited by the classical Abbe-Rayleigh diffraction criterion, spatial resolution of a far-field instrument cannot be better than about a half of the wavelength of the incident light. Thus conventional spectral imaging techniques based on, e.g., Fourier transform infrared (FTIR), Raman, and the emerging THz time-domain spectroscopies, are not directly applicable to characterize samples with an ultra-high spatial resolution. This has greatly impeded progress toward in-depth understanding of materials' and devices' electromagnetic properties at the nano-/micro- scale. Therefore, there has been a continuous and pressing need for instruments with a high spatial resolution to circumvent the diffraction limitation. This has driven the substantial effort in the innovation and development of many types of near-field spectroscopic imaging instruments to reach spatial resolutions well beyond the diffraction limit. Amongst these near-field techniques, the scattering-type scanning near-field optical microscopy (s-SNOM) is an outstanding representative, due to its unprecedented super spatial resolution. S-SNOM has attracted tremendous attention as a useful tool for examining the chemical and/or physical properties of biological, organic and inorganic samples at the micro/nano scale, such as the fingerprint spectra of proteins and viruses [1], [2], carrier distribution of micro/nano semiconductor devices [3]–[5], and localized electromagnetic responses of metamaterials and devices [6], [7].

In a typical s-SNOM, a nano- or micro-sharp tip, serving as the antenna for the near-field optical microscope, is crucial for achieving an ultra-high spatial resolution because it can help produce the so-called tip-enhanced electric field around its apex to circumvent the diffraction limit of optical waves, and the resolution of s-SNOM is defined by the tip's sharpness and independent of the incident wavelength. In addition, in order to effectively extract the near-field signal buried in the background noise, the scattered signal of the tip is usually modulated by an imposed tip oscillation at a certain frequency; and a lock-in detection technique is employed to extract the near-field signal by suppressing the background noise [8], [9].

In recent years, s-SNOM has been applied successfully in the visible, infrared, and terahertz (0.6 - 8.5 THz) regions of the electromagnetic spectrum [7], [10]–[13], while not yet

The associate editor coordinating the review of this manuscript and approving it for publication was Shah Nawaz Burokur.

available in the millimeter wave (mmW) region because of the serious mismatch between the wavelength and tip length. Attempts at coupling commercial s-SNOM with an mmW source have invariably failed, because the standard tip is too short (generally between 4-20 μm) to be used to enhance the localized electric field according to standard antenna theory [14], [15], whereas long tips suitable for enhancing mmW field cannot be used with currently available scanning probe microscopy (SPM) for imaging due to inherent configuration limits. To overcome this technical barrier, a variety of aperture based or apertureless near-filed tips/probes were developed, such as low-loss dielectric material sharpened pyramidal tip with a micron-sized plane facet [16], polymethylmethacrylate rectangular tapered probe with metal coating [17], quartz (dielectric) probes excited with a horn antenna [18], Teflon probe azimuthally patterned with several copper strips [19], and microfabricated resonant micro stripline probe [20]. However, none of them was capable of achieving a resolution better than 1 μm in the mmW region. On the other hand, in the microwave regime there has been available for some time a type of commercial instrument named scanning microwave microscopy (SCM) that can map samples with resolution of tens of nanometers, albeit at a fixed frequency of a few GHz. Here the tip is a part of the assembly of a high-Q microwave resonator, which supplies the locally enhanced field required for near-field imaging at the resonance. In conjunction with a vector network analyzer, a SCM can readily map the S-parameters to obtain the various sample properties, such as impedance/capacitance, dielectric constants, and dopant density distribution [21]–[23]. However, the microwave resonator based near-field enhancement strategy can hardly be replicated in the mmW band, as such a resonator is either unavailable or impractical. There have been reports of using a long metal wire as the tip antenna in an s-SNOM, and achieving a sub-micrometer resolution in the THz band [24], [25]. However, since the tip was kept at a constant height above the sample surface during scan, the signal to noise ratio was marginal, and high-resolution near-field signal could only be detected by a liquid helium cooled bolometer, which is quite complicated and expensive to operate.

To circumvent the intrinsic technical difficulties described above, we designed and homebuilt a W-band microscope based on a continuous wave W-band source operating at 110 GHz. In this system, the tip's length and curvature radius are 6 mm and 0.89 μm respectively, both being 2 orders of magnitude larger than those of standard AFM tips, in order to further enhance the localized electric-field in the near-field region. The tip is dithered vertically, and the near-field signal is demodulated at a harmonic of the dithering frequency to suppress the background noise effectively. A spatial resolution of $\sim 1\mu$m has been achieved which is about 1/3000 of the incident wavelength, at a workable signal to noise ratio (23.8 dB). Thus apart from demonstrating a simple, easy to operate, yet robust W-band near-field scanning microscope, the essential technical improvements the new microscope embodies should be useful in solving the bottleneck problems in further development of microwave and mmW s-SNOM technology.

II. EXPERIMENTAL CONFIGURATION AND FDTD SIMULATION

A. SYSTEM SET-UP

Our experimental system was built on a 110 GHz radiation source, using frequency multiplication. The schematic configuration of the experimental set-up is shown in Fig. 1. Briefly, a seed signal source at 27.5 GHz delivers the signal to two tandem frequency doublers, D1 and D2 (Virginia Diodes, Inc) after the signal amplification with a power amplifier, with the resulting 110 GHz radiation wave (with power of 30 mW) transmitted to free space by a horn antenna, and focused to a stainless steel tip by an oversized parabolic mirror. The tip is driven by a piezo actuator (Physik Instrumente, Germany) through a servo-control module to oscillate together with the piezo at a frequency of Ω (chosen to be 400 Hz here), with an amplitude of 2 μm, reminiscent of the tapping mode of an atomic force microscopy (AFM). The scattered radiation is detected with a quasi-optical Schottky diode (ACST, Germany). A conventional coaxial optical microscope is placed at the side of the tip to monitor the tip-sample distance [26].

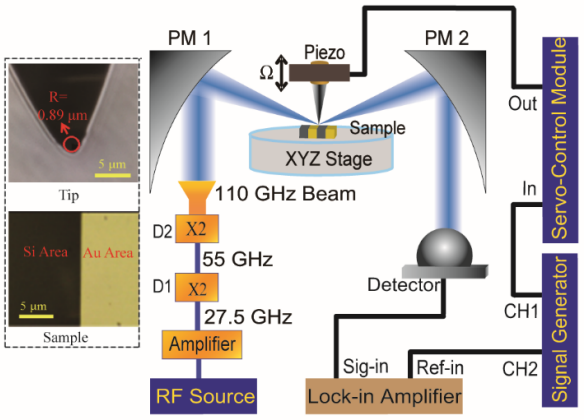

FIGURE 1. Configuration of the millimeter wave near-field microscope. A 110 GHz beam is emitted from the horn antenna, and focused on the tip apex by a parabolic mirror (PM1). The scattered light containing the sample information is collected by PM2 and directed to the far-field detector. The signals used to drive the tip and to provide the input reference for the lock-in amplifier are introduced from the same signal generator through channels CH1 and CH2, respectively. Optical microscopic images on the left show the tip and the sample, respectively.

In the experiment, an Au-Si periodic grating was used as the standard sample, with the Au region having 50 nm thick Au film evaporated on a Si substrate. The sample was placed on a high-precision three-dimensional stage which can move with a minimum step of 4 nm in scanning. The signal generator (Tektronix, USA) provided two output signal channels, i.e., the signal from channel 1 (CH1) was employed as the source to drive the piezo resonator, and that from channel 2 (CH2) was used as the reference input of the lock-in amplifier (Zurich Instruments, Switzerland), respectively.

This configuration ensures that all the signals needed for the analysis are well synchronized, which is necessary for the accurate extraction of near-field information.

B. TIP-SAMPLE SEPARATION CONTROL

Tip-sample separation means the smallest distance between the tip apex and sample surface during the scanning. According to commonly accepted understanding, the separation between the tip and the sample under test should be kept as small as possible to obtain a stronger enhanced electric-field [24]. Therefore, it is crucial to keep the tip-sample separation within the scale of micrometer during the scanning to collect the high-resolution near-field signal. Since the tip can be easily damaged if it inadvertently crashes onto the sample surface, an effective means for precise control of the tip-sample separation is essential in the near-field measurement of samples. Without a closed-loop feedback mechanism for such distance control, in contract to AFM based systems where force feedback can be relied upon, or STM's where tunnel current plays the role of feedback, we used a high-resolution coaxial microscope which is coupled with a CCD camera and sideway-aligned with the tip-sample system to obtain the microscopic image of the tip apex and sample surface, as shown in Fig. 2. During scanning, with the assistance of a cold light source lighting up the near-filed region, the microscopic image of the tip and sample surface could be easily obtained by the CCD camera to calculate the tip-sample separation and avoid collision. It should be pointed out that the piezo-actuator employed in our system possesses the properties of high stiffness and high linearity, and its nonlinearity can be kept well below 0.01% within the travel range of 10μm. Such excellent mechanical precision of the piezo-actuator, plus the adequate rigidity of the stainless steel needle, helps insure that the mmW microscopic image of the tip provides the positional information and the tip-sample separation accurately.

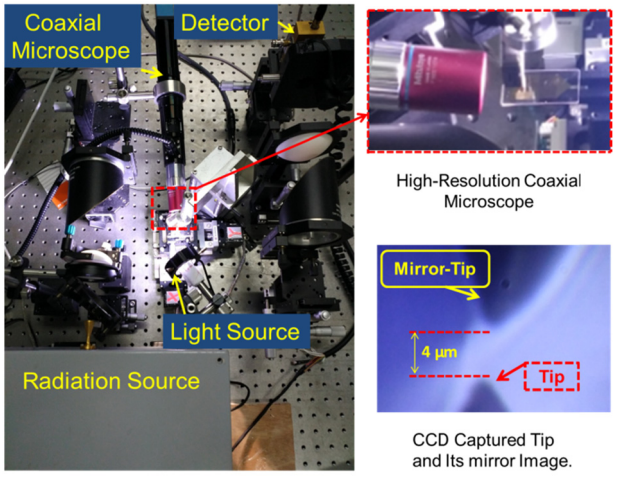

FIGURE 2. Configuration of the near-field microscope. Top right corner: partially enlarged detail of the coaxial microscope. Lower right corner: the tip and its mirror image obtained by the CCD camera.

The method described above has proved to be quite effective in controlling and measuring the tip-sample separation and has achieved a reasonable success rate during our series of experiments. However, this method is somewhat tricky to execute because of the complicated procedures and severe damage penalties. The smallest tip-sample separation we could control accurately was 0.5 μm during scanning, limited mainly by the magnification factor of the microscope used. More fundamentally, due to the lack of a closed-loop feedback mechanism in the present system, the technical errors, such as the oscillation amplitude error, the xyz-stage position drift, and the calibration error may introduce substantial deviations into the results, and may lead to tip-sample's inadvertent crashes if too small a tip-sample separation was set. For the system under consideration, a tip-sample separation of 0.5 μm seemed to be a good compromise between caution and accuracy.

C. SIMULATION AND ANALYSIS OF ANTENNA LENGTH

According to the standard antenna theory, the incident field can be strongly enhanced by the antenna when its length is around an integral multiple of half wavelength ($\lambda/2$) of the incident wave [14], [15]. In order to obtain an optimized antenna length, we carried out finite-difference time-domain (FDTD) electromagnetic simulations to ascertain and quantify the resonant effects by choosing 1.5 mm ($\lambda/2$), 3 mm (λ) and 6 mm (2λ) as the shaft length of the tip. The simulation results are shown in Fig. 3.

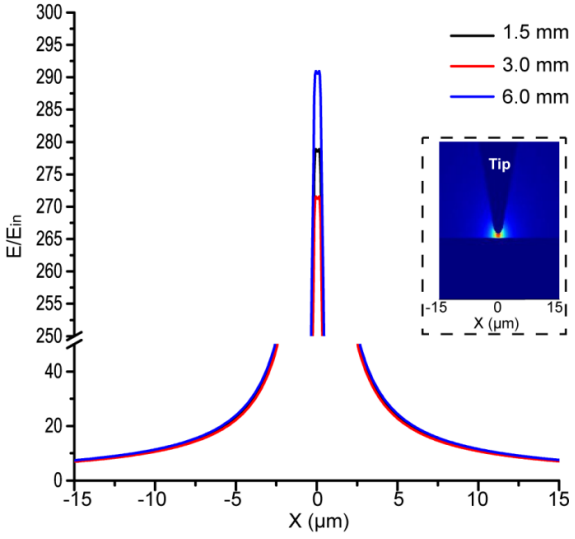

FIGURE 3. FDTD simulation of the electric-field distribution in the vicinity of a perfect electrical conductor along the X direction for various antenna lengths (black line, 1.5 mm; red line, 3.0 mm; and blue line, 6.0 mm). The inset shows the alignment of the tip in the simulation. The elevation angle of the incident wave is 60 degrees relative to the tip axis.The tip-substrate separation is 500 nm. E_{in} and E stands for the incident electric field and simulated electric-field, respectively.

From Fig. 3, it is evident that the antenna with a length of 6 mm has the strongest field enhancement effect; therefore the tip with a shaft length of 6 mm was used in our subsequent experiments. Based on the lightning-rod-effect theory and

related experimental evidences, the enhanced field is mainly confined to the region around the tip apex, on the scale of the radius of curvature of the tip apex. This enhanced field is normally termed the ''near-field'' that decays exponentially with the tip-sample separation [27], [28]. In our experiment the radius of curvature of the tip apex is 0.89 μm, so the enhanced electric field is only significant within a distance of $\sim 1\mu$m around the tip apex.

D. SIMULATION OF TIP-ENHANCED FIELD

To obtain detailed information on the distribution of the near field and provide a practical guidance for experiments, we established an FDTD model mimicking the experimental condition to perform simulations for the situation of a tip above an Au film (tip-Au) and above a Si substrate (tip-Si), respectively. The near-field distributions of the tip-Au case for three different tip-sample separations (0.5 μm, 1.0 μm and 1.5 μm) are shown in Fig. 4. We note that the results for the corresponding tip-Si cases with different tip-sample separations are very similar to the tip-Au cases, except that the near-field strengths are lowered by an overall factor of about 35%. Thus in the interest of brevity the tip-Si results are not displayed here.

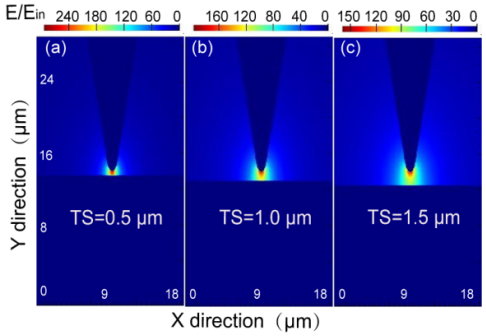

FIGURE 4. FDTD simulation of the electric field distribution of a tip above a gold film with different tip-sample separations (TS). (a) 0.5 μm, (b) 1.0 μm and (c) 1.5 μm. The radius of tip is 0.9 μm. The elevation angle of the incident wave is 60 degrees relative to the tip axis.

From the simulation result shown in Fig. 4, it can be obtained that the incident electric field is magnified by up to 300 times in the near-field region. Such an enhancement is due to the combination of several mechanisms. The most important mechanism is the so-called lightning-rod effect, originated from the concentration of charge on the tip of a rod and the concentrated electric field lines in the immediate vicinity of the tip; another mechanism is the polarization or image charge induced in the sample or substrate by the tip charge, which acts to intensify the electric field; and last but not least, the resonant excitation between the tip and the incident field can enhance the electric field near the tip apex when the length of the tip satisfies the well-known wavelength-antenna length resonant relation [29]. The first two effects are strongly dependent on the tip-sample separation, i.e., the closer the separation the stronger the enhancement. This is clearly borne out in Fig. 4(a)-(c), where it is readily seen that the enhanced electric field is concentrated around the tip apex more effectively when the tip-sample separation is smaller. The enhanced field around the tip apex decays quickly with the increase of the tip-sample separation on the scale of the curvature radius of the tip apex, but the decay is tempered somewhat beyond this specified region. Thus apart from a judicious selection of the tip length and a sharp tip apex, it is paramount to have the tip operating as close as possible to the sample surface to ensure the strongest interaction between the tip and the sample.

E. DIFFERENCES AND SIMILARITIES BETWEEN THE PRESENT SYSTEM AND CONVENTIONAL S-SNOM

There are many differences and similarities between our home-built system and the conventional s-SNOM. Both of them are based on the premises of lightning-rod effect around the tip apex and detecting the near-field signal arising from the localized enhanced sample-relevant electric-field in the far-field region. However, the conventional s-SNOM is mostly based on AFM, in which standard commercial cantilevered tips were used, with a typical tip shaft length of 4-20 μm and vertical oscillation amplitude of several tens or hundreds of nanometers. According to our simulations above and the standard antenna theory, in order to obtain a strong field enhancement, the length of the antenna, i.e., the tip shaft length, should be an integral multiple of the half wavelength of incident waves. Thus standard commercial tips can be employed to achieve a good field enhancement in visible, infrared, and even high THz frequency spectral regions, but not in the low THz frequency region and millimeter wave band.

In our W-band microscope, the radiation source works at 110 GHz ($\sim$3 mm wavelength), which determines that the tip's length should be at least 1.5 mm. We designed and made tips with various lengths according to the need of our experiments, to receive, localize and enhance the incident electric-field of the 110 GHz wave. Based on the simulation results shown in Fig. 3, we chose the tip with a length of 6 mm for our experiments, a length of 2 orders of magnitude longer than the tips used in the conventional s-SNOM and SCM. The curvature radius of the tip is 0.89 μm that is also 2 orders of magnitude larger than that of conventional s-SNOM tips.

Compared with the conventional SPM based near-filed systems, the tip in our W-band microscope does not rise or fall following the surface topography due to the lack of a feedback function in the vertical direction, thence no topographic image can be obtained in our experiments.

III. EXPERIMENTAL RESULTS AND ANALYSIS

A. RESOLUTION TESTED IN THE CASE OF DIFFERENT HARMONICS AND TIP-SAMPLE SEPARATIONS

To test the performance of our near-field system built based on a self-homodyne detection technique (Fig. 1), we conducted experiments by scanning the Au-Si boundary of a grating. Since near-field signals extracted at a higher harmonic

of the tip oscillation frequency (Ω) is very helpful to obtain pure near-field signals and suppress background noises [30], [31], we applied a lock-in detection technique to extract the near-field signal at the second (2Ω) and third harmonic frequency (3Ω), respectively. A scanning step increment of 4 nm was used in the scanning process to collect the data of near-field signals, with about 20k points recorded along a single scanning line. Only the data recorded in a distance of 30 μm across the Au-Si boundary are displayed in Fig. 5 for the analysis and demonstration of the spatial resolution of the system.

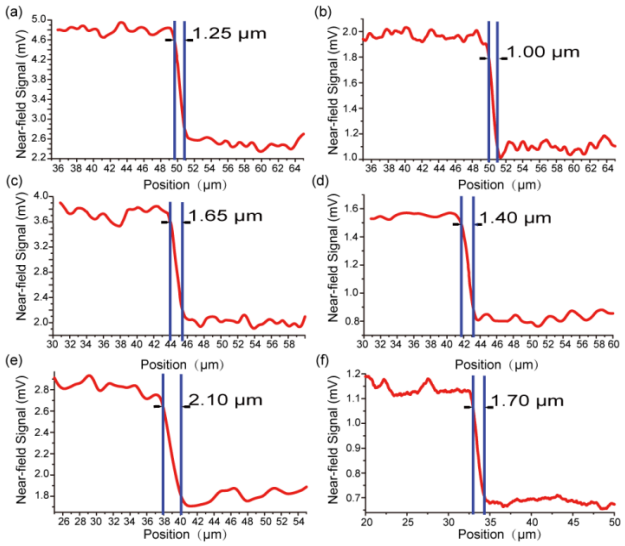

FIGURE 5. Transition of 110 GHz near-field signal at the Au-Si boundary. Tip-sample separations are 0.5 μm for (a) and (b), 1.0 μm for (c) and (d), and 1.5 μ m for (e) and (f). The signal demodulated at 2Ω for (a), (c) and (e), and 3Ω for (b), (d) and (f). Ω represents the fundamental oscillation frequency of the tip. The vertical solid lines correspond to 90% and 10% of the averaged signal difference between the signals collected on Au and Si substrates. The distance between the two solid lines indicates the spatial resolution of the microscope. The tip-sample separation is the distance between the lowest point of the tip apex during oscillation and the sample surface. The elevation angle of the incident wave is 60 degrees relative to the tip axis.

It can be observed from Fig. 5 that both the tip-sample separation and the harmonics demodulated are important factors for achieving high spatial resolution. At 2Ω (Fig. 5(a), (c) and (e)), the resolution of the system decreased from 1.25 μm to 2.10 μm when the separation was increased from 0.5 μm to 1.5 μm. At 3 Ω (Fig. 5(b), (d) and (f)), the resolution of the system decreased from 1.0 μm to 1.7 μm when the separation was increased from 0.5 μm to 1.5 μm. The results suggest that smaller tip-sample separation and higher harmonics are beneficial to a better near-filed spatial resolution. The influence of the tip-sample separation on the spatial resolution can be interpreted by considering that the larger the tip-sample separation is, the weaker the tip-induced sample polarization that can strengthen the local near-field will be [28]. The spatial resolution of the near-field signal demodulated at 3Ω is better than that demodulated at 2Ω can be ascribed to that the extraction of the near-field signal at 3Ω is more effective than 2Ω to suppress the background noises for a self-homodyne detection technique used in our experiments [8], [30], [32]. A spatial resolution of 1 μm ($\sim \lambda/3000$) has been achieved when the tip-sample separation was adjusted down to 0.5 μm and the near-field signal was extracted at 3Ω. In this case, an acceptable signal-to-noise ratio (SNR) of 23.8 dB and signal error within 10% of the near-field signal can be realized. The signal error is very likely caused by the remaining background noise as well as the stability of the piezo resonator.

B. SIGNAL QUALITY AND STABILITY

In terms of signal strength alone, demodulation at the fundamental frequency would have resulted in the strongest signal. However, due to scattering from the substrate surface and the tip shaft, which overwhelms the true near field scattering off the tip apex and its immediate neighborhood, demodulations at higher order harmonics which carry mostly near-field information are obviously better choices. In Table 1, we list the SNR for the three tip-sample separations for both the gold substrate and the silicon substrate, with the 2nd and 3rd harmonic demodulation based signal detection scheme.

TABLE 1. SNR of near-field signal for Tip-Au/ Tip-Si cases and different tip-substrate (TS) separations.

	SNR of 2Ω (dB)		SNR of 3Ω (dB)	
TS	Au Area	Si Area	Au Area	Si Area
0.5μm	28.7	23.3	23.8	18.5
1.0μm	26.1	21.2	21.4	16.2
1.5μm	23.9	20.0	18.7	14.2

The observation of using higher harmonic frequency demodulation does not result in the best SNR in our experiment is consistent with earlier observations [8], [33]. This phenomenon can be attributed to an excessive higher-frequency attenuation suffered by the demodulated signal during the lock-in process [32], which affects the phase of the near-field signal and background noise differently. A more in-depth understanding can be obtained through the relation $I = A\cos(\phi_s)+B\cos(\phi_s\text{-}\phi_b)$, ($I$ stands for the intensity of the detected signal, A and ϕ_s are the amplitude and phase related to near-field-signal's Fourier series respectively, B and ϕ_b are the amplitude and phase of the background noise respectively), and ϕ_s can differ with different harmonic frequencies. Therefore, the phase value can influence the signal intensity directly, and may further induce the observed effect mentioned above. We have discussed this mechanism in detail elsewhere [30].

Based on our analysis, the near-field signal jitters at the Au and Si area shown in Fig. 5 can also be partly attributed to the oscillation precision of the piezo actuator, in addition to the deviations introduced by the background signal scattered from the sample surface and the tip shaft. To investigate the stability of the near-field signals recorded under various

experimental conditions, we calculated the standard deviations (SD) of the signal, as listed in Table 2. There are no big differences between the SDs of the signals measured above the Au Area and the Si area, which is expected because the near-field signal jitters (variations) at harmonic frequencies (2Ω and 3Ω) are mainly related to the precision of the piezo actuator. Certainly, the jitters could also be related to topological features on the substrate surface if the sample surface is not smooth enough, which is not the case for our experiments.

TABLE 2. SD of near-field signals for Tip-Au/ Tip-Si AT different TS separations.

	SD of 2Ω (mV)		SD of 3Ω (mV)	
TS	Au Area	Si Area	Au Area	Si Area
0.5μm	0.289	0.245	0.100	0.092
1.0μm	0.221	0.239	0.081	0.107
1.5μm	0.147	0.111	0.045	0.034

From Table 2, we can see that the SD values of the 3Ω signals are smaller than those of the 2Ω signals, indicating that demodulation at 3Ω is more effective than 2Ω in improving the signal stability. The results well demonstrate that extracting the near-field signal at a higher harmonic frequency can commendably suppress the unstable background noise and thus improve the signal's stability.

To provide further support for this conclusion, we examined the demodulated signals at Au surface as a function of tip-sample separation and made a comparison with the corresponding simulated results, as shown in Fig. 6.

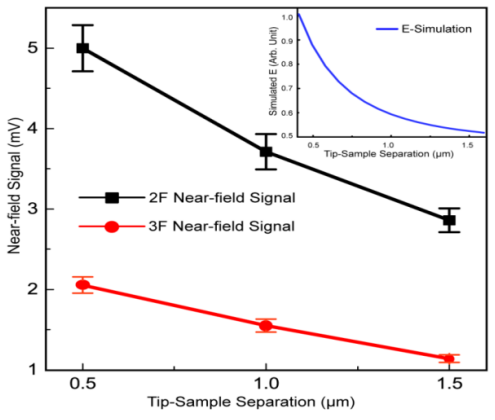

FIGURE 6. Demodulated signals at 2nd(2F) and 3rd(3F) harmonics as functions of tip-sample separation. Inset: Scattered electric-field strength as a function of the tip-sample separation obtained from simulation.

From Fig. 6, we observe that the general trends of the 2Ω and 3Ω signals evolving with tip-sample separation are similar, and both are essentially in agreement with that of theoretical calculation, which provides convincing evidence that background noises mixed in the demodulated signals are suppressed effectively. Also, not surprisingly, we observe that the error bars on the 2Ω data are much bigger than those of the 3Ω counterparts, even though the former has much higher overall signal strength, consistent with our earlier discussion.

An experimental phenomenon beyond our original expectation is that the SD values basically decrease with the increase of tip-sample separation (TS) at both 2Ω and 3Ω, i.e., larger TS gives rise to smoother signal. After careful consideration, we conclude that it also resulted from the effect of oscillation precision of the piezo actuator, as we described above. TS directly determines the strength of the enhanced near-field signal, and when TS is on the scale of the curvature radius of the tip apex, there is an intense interaction between the tip apex and the sample; and naturally, the deviation of oscillation will induce relatively large jitters to the field strength and lead to signal jitters. However, when TS is beyond the tip apex scale, the enhanced field effect becomes insignificant, so the influence of oscillation-precision on the signal intensity diminishes. In the case of high harmonic frequency demodulation, the influence of the background noise has been restricted severely by the lock-in amplifier, the effect of oscillation deviation becomes relatively large, and thus small TS entails a more noticeable SD than the case of large TS.

C. DEVIATION ANALYSIS

It is worthwhile to emphasize that although the Au surface is 50 nm higher than the Si surface in the grating, this height difference has no obvious influence on our experimental results. When performing the experiments shown in Fig. 5, we have deliberately deviated the tip-sample position from the target position (0.5 μm, 1 μm and 1.5 μm) by $\pm$ 50 nm, the obtained near-field signal shows nearly no change, either above the Au surface or the Si surface. This result is understandable by considering that the radius of curvature of the tip (0.89 μm) and the wavelength of the incident light ($\sim$ 3 mm) are much larger than 50 nm. To further confirm this conclusion, we simulated the electric-field distribution above the Au/Si surface along the tip shaft axis direction, with an increment of 50 nm and 100nm for the maximum TS of 0.5 μm and 1.0 μm, respectively, and plotted the simulation results as bar graphs, as shown in Fig.7.

From Fig. 7, it can be seen that the enhanced electric field/near-filed signal changes very slowly along the tip shaft axis direction for any of the two tip-sample separations (0.5 μm and 1 μm), no matter the tip was positioned above the Au surface or the Si surface. When the tip-sample separation was set to 0.5 μm or 1 μm, a distance change of 50 nm along the tip shaft axis direction can only lead to a very small change in the near-field signal, which is calculated to be less than 3% of the maximum signal (the left-most bar in Fig. 7 (a) and (b)). The simulation is highly consistent with our experimental results, further confirming that the influence of the height difference (50 nm) between the Au surface and Si surface on the near-field signal is negligible in our case.

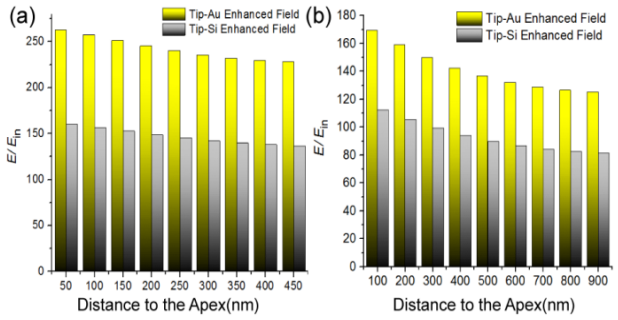

FIGURE 7. FDTD simulated enhanced electric field strength along the tip shaft axis direction as a function of distance from the tip apex towards the substrate (Au/Si), with the origin set at the tip apex, for tip-sample separations of (a) 0.5 μm and (b) 1.0 μm, respectively. The parameters of the simulation are same as that of Figure 4.

IV. CONCLUSION

In summary, we have presented a home-built scattering type scanning millimeter wave microscope based on a 110 GHz CW radiation source and demonstrated a resolution of 1.0 μm ($\sim \lambda/3000$), with a SNR of 23.8 dB, under standard ambient conditions. The system is demonstrated as a promising tool for imaging near-field microscopic features in W-band, and it may pave the way for further development of practical mmW and microwave near-field spectral imaging instruments.

REFERENCES

[1] F. Ballout *et al.*, "Scanning near-field IR microscopy of proteins in lipid bilayers," *Phys. Chem. Chem. Phys.*, vol. 13, no. 48, pp. 21432–21436, 2011.
[2] I. Amenabar *et al.*, "Structural analysis and mapping of individual protein complexes by infrared nanospectroscopy," *Nature Commun.*, vol. 4, no. 4, p. 2890, 2013.
[3] J. N. Chen *et al.*, "Optical nano-imaging of gate-tunable graphene plasmons," *Nature*, vol. 487, no. 7405, pp. 77–81, Jul. 2012.
[4] A. J. Huber, F. Keilmann, J. Wittborn, J. Aizpurua, and R. Hillenbrand, "Terahertz near-field nanoscopy of mobile carriers in single semiconductor nanodevices," *Nano Lett.*, vol. 8, no. 11, pp. 3766–3770, 2008.
[5] J. M. Stiegler *et al.*, "Nanoscale free-carrier profiling of individual semiconductor nanowires by infrared near-field nanoscopy," *Nano Lett.*, vol. 10, no. 4, pp. 1387–1392, Apr. 2010.
[6] Z. Fei *et al.*, "Gate-tuning of graphene plasmons revealed by infrared nano-imaging," *Nature*, vol. 487, no. 7405, pp. 82–85, Jul. 2012.
[7] M. Schnell, P. S. Carney, and R. Hillenbrand, "Synthetic optical holography for rapid nanoimaging," *Nature Commun.*, vol. 5, p. 3499, Mar. 2014.
[8] T. Taubner, F. Keilmann, and R. Hillenbrand, "Effect of tip modulation on image contrast in scattering-type near-fieldoptical microscopy," *J. Korean Phys. Soc.*, vol. 47, pp. S213–S216, Aug. 2005.
[9] M. Brehm *et al.*, "Consolidating apertureless SNOM," *J. Korean Phys. Soc.*, vol. 47, pp. S80–S85, Aug. 2005.
[10] R. Hillenbrand and F. Keilmann, "Complex optical constants on a subwavelength scale," *Phys. Rev. Lett.*, vol. 85, no. 14, pp. 3029–3032, Oct. 2000.
[11] E. Yoxall, M. Schnell, S. Mastel, and R. Hillenbrand, "Magnitude and phase-resolved infrared vibrational nanospectroscopy with a swept quantum cascade laser," *Opt. Express*, vol. 23, no. 10, pp. 13358–13369, May 2015.
[12] C. Liewald, S. Mastel, J. Hesler, A. J. Huber, R. Hillenbrand, and F. Keilmann, "All-electronic terahertz nanoscopy," *Optica*, vol. 5, no. 2, pp. 159–163, 2018.
[13] F. Kuschewski, H.-G. V. Ribbeck, J. Döring, S. Winnerl, L. M. Eng, and S. C. Kehr, "Narrow-band near-field nanoscopy in the spectral range from 1.3 to 8.5 THz," *Appl. Phys. Lett.*, vol. 108, no. 11, p. 97, 2016.
[14] A. Alù and N. Engheta, "Input impedance, nanocircuit loading, and radiation tuning of optical nanoantennas," *Phys. Rev. Lett.*, vol. 101, no. 4, 2008, Art. no. 043901.
[15] A. Alù and N. Engheta, "Tuning the scattering response of optical nanoantennas with nanocircuit loads," *Nature Photon.*, vol. 2, no. 5, pp. 307–310, 2008.
[16] N. Klein, P. Lahl, U. Poppe, F. Kadlec, and P. Kužel, "A metal-dielectric antenna for terahertz near-field imaging," *J. Appl. Phys.*, vol. 98, no. 1, Jul. 2005, Art. no. 014910.
[17] B. Zhu *et al.*, "Resolution analysis of a polymethylmethacrylate tapered probe in near-field terahertz imaging," *Appl. Comput. Electromagn. Soc. J.*, vol. 30, no. 1, pp. 30–41, Jan. 2015.
[18] O. C. Fawole and M. Tabib-Azar, "Terahertz near-field imaging of biological samples with horn antenna-excited probes," *IEEE Sensors J.*, vol. 16, no. 24, pp. 8752–8760, Dec. 2016.
[19] T.-J. Huang, H.-H. Tang, L.-Z. Yin, J.-Y. Liu, Y. Tan, and P.-K. Liu, "Experimental demonstration of an ultra-broadband subwavelength resolution probe from microwave to terahertz regime," *Opt. Lett.*, vol. 43, no. 15, pp. 3646–3649, Aug. 2018.
[20] O. Benzaim, K. Haddadi, M. M. Wang, A. Maazi, D. Glay, and T. Lasri, "Scanning near-field millimeter-wave microscope: Application to a vector-coding technique," *IEEE Trans. Instrum. Meas.*, vol. 57, no. 11, pp. 2392–2397, Nov. 2008.
[21] B. Knoll, F. Keilmann, A. Kramer, and R. Guckenberger, "Contrast of microwave near-field microscopy," *Appl. Phys. Lett.*, vol. 70, no. 20, pp. 2667–2669, 1997.
[22] B. T. Rosner and D. W. van der Weide, "High-frequency near-field microscopy," *Rev. Sci. Instrum.*, vol. 73, no. 7, pp. 2505–2525, 2002.
[23] V. V. Zavyalov, J. S. McMurray, and C. C. Williams, "Advances in experimental technique for quantitative two-dimensional dopant profiling by scanning capacitance microscopy," *Rev. Sci. Instrum.*, vol. 70, no. 1, pp. 158–164, Jan. 1999.
[24] H.-T. Chen, R. Kersting, and G. C. Cho, "Terahertz imaging with nanometer resolution," *Appl. Phys. Lett.*, vol. 83, no. 15, pp. 3009–3011, 2003.
[25] H.-T. Chen, S. Kraatz, G. C. Cho, and R. Kersting, "Identification of a resonant imaging process in apertureless near-field microscopy," *Phys. Rev. Lett.*, vol. 93, no. 26, 2004, Art. no. 267401.
[26] G. Geng *et al.*, "Imaging brain tissue slices with terahertz near-field microscopy," *Biotechnol. Prog.*, to be published.
[27] B. Knoll and F. Keilmann, "Enhanced dielectric contrast in scattering-type scanning near-field optical microscopy," *Opt. Commun.*, vol. 182, nos. 4–6, pp. 321–328, 2000.
[28] A. Cvitkovic, N. Ocelic, and R. Hillenbrand, "Analytical model for quantitative prediction of material contrasts in scattering-type near-field optical microscopy," *Opt. Express*, vol. 15, no. 14, pp. 8550–8565, 2007.
[29] *Nature*, vol. 179, no. 4567. Hoboken, NJ, USA: Wiley, 1957, pp. 947–947.
[30] G. Dai *et al.*, "Signal detection techniques for scattering-type scanning near-field optical microscopy," *Appl. Spectrosc. Rev.*, vol. 53, no. 10, pp. 1–30, 2018.
[31] F. Keilmann and R. Hillenbrand, "Near-field microscopy by elastic light scattering from a tip," *Philos. Trans. Roy. Soc. London A, Math., Phys. Eng. Sci.*, vol. 362, no. 1817, pp. 787–805, 2004.
[32] S. Mastel, A. A. Govyadinov, C. Maissen, A. Chuvilin, A. Berger, and R. Hillenbrand, "Understanding the image contrast of material boundaries in IR nanoscopy reaching 5 nm spatial resolution," *ACS Photon.*, vol. 5, no. 8, pp. 3372–3378, 2018.
[33] L. Gomez *et al.*, "Apertureless scanning near-field optical microscopy: A comparison between homodyne and heterodyne approaches," *J. Opt. Soc. Amer. B, Opt. Phys.*, vol. 23, no. 5, pp. 823–833, May 2006.

GUANGBIN DAI received the B.S. degree from Changchun Institute of Technology in 2013. He is currently pursuing the Ph.D. degree with the College of Instrumentation and Electrical Engineering at Jilin University, Changchun, China and is also a guest student at Chongqing Institute of Green and Intelligent Technology, Chinese Academy of Sciences.

His main research interests include terahertz and millimeter wave imaging, near-field instruments, terahertz spectroscopy and terahertz microscopy.

GUOSHUAI GENG received the B.S. degree in electrical engineering and the M.S. degree in instrument science and electrical engineering from Jilin University, Changchun, China, in 2015 and 2018, respectively.

His main research interests include digital image processing, near-field imaging, and terahertz spectral imaging.

XIAOXUAN ZHANG received the B.S. degree from the School of Electro-Mechanical Engineering, Qingdao University, in 2015. She is currently pursuing the Ph.D. degree with the College of Instrumentation and Electrical Engineering, Jilin University, Changchun, China.

Her research interests include 3-D terahertz tomographic imaging radar and nondestructive detection of defects in materials.

JIE WANG received the B.S. degree in electrical engineering from Jilin University, Changchun, China, in 2017, where she is currently pursuing the M.S. degree in instrument science and electrical engineering.

Her main research interests include terahertz imaging algorithm and the detection of defects in composite materials.

TIANYING CHANG received the Ph.D. degree from the College of Control Science and Engineering, Shandong University, Jinan, China, in 2009. From 2007 to 2008, she was a joint Ph.D. candidate at the Stevens Institute of Technology. After graduation, she was a Lecturer with Shandong University and a Postdoctoral Research Associate with New York University. She is currently an Associate Professor with Jilin University. Her research interests include optical fiber sensors, THz systems, and nano-optics.

HONG-LIANG CUI received the Ph.D. degree in theoretical condensed matter physics from the Stevens Institute of Technology, in 1987.

He was a Professor of applied and engineering physics with the Stevens Institute of Technology and New York University. He is currently a Professor with the College of Instrumentation and Electrical Engineering, Jilin University, and the Chongqing Institute of Green and Intelligent Technology, Chinese Academy of Sciences. His research interests include solid-state electronics, fiber optical communications and sensing, high-frequency electromagnetic wave propagation and interaction with matter, and high-performance computing approaches to the modeling of semiconductor and molecular devices and phenomena.